Graphical Analysis of Electrochemical Impedance Spectroscopy of Two Consecutive Irreversible Electron Transfers. 2. Zinc Anodic Dissolution in Acid Media

J. J. García-Jareño,[†] D. Giménez-Romero,[†] M. Keddam,[‡] and F. Vicente*,[†]

Departament de Química Física, Universitat de València, C/Dr Moliner, 50, 46100, Burjassot, València, Spain, and UPR 15 CNRS, Laboratoire des Interfaces et Systèmes Electrochimiques (LISE), Université P. et M. Curie, 4 place Jussieu, F-75252 Paris Cedex 05, France

Received: July 20, 2004; In Final Form: November 25, 2004

The graphical analysis of the impedance plots is used in the study of the electrodic systems that take place through two consecutive single electron transfers. The zinc anodic dissolution is studied by using this procedure. The characteristic points easily allow us to explain and to simulate the impedance behavior of this electrodic system according to the steady-state potential and the roughness of the working electrode. The direct procedure for parametrical identification from the graphical analysis allows us to reduce the time needed for an impedance experiment. This graphical analysis is suggested for studying thin coated galvanized steels.

Introduction

A technique for graphical analysis based on the exploitation of a limited number of characteristic points for the impedance spectrum was developed in part 1 of this work (Figure 1).[1]

Like for many metals, the zinc anodic dissolution in acid media could be described through two consecutive single electron transfers followed by a heterogeneous irreversible process, which implies the mass transfer from the surface to the solution, in some experimental conditions[2,3]

$$\mathrm{Zn}\,(\Gamma_0) \xrightarrow{k_1} \mathrm{Zn^I}\,(\Gamma_1) + 1\mathrm{e}^- \quad \text{(i)}$$

$$\mathrm{Zn^I}\,(\Gamma_1) \xrightarrow{k_2} \mathrm{Zn^{II}}\,(\Gamma_2) + 1\mathrm{e}^- \quad \text{(ii)}$$

$$\mathrm{Zn^{II}}\,(\Gamma_2) \xrightarrow{k_3} \mathrm{Zn^{2+}}\,(\Gamma_2) \quad \text{(iii)}$$

Accordingly, in these experimental conditions, the theoretical faradaic impedance function of this electrochemical system can be expressed by means of the following expression.[1]

$$FA\frac{\mathrm{d}E}{\mathrm{d}i} = \frac{(-\omega^2 + R)(S + T\omega^2) + Y\phi\omega^2}{\omega^2\phi^2 + (T\omega^2 + S)^2} + j\frac{(TY + \phi)\omega^3 + \omega(SY - \phi R)}{\omega^2\phi^2 + (T\omega^2 + S)^2} \quad (1)$$

$$R = (k_2^0 + k_1^0)k_3 + k_1^0 k_2^0 \quad (2)$$

$$S = ((k_2^0 + k_1^0)k_3 + k_1^0 k_2^0)(k_1^0 b_1\overline{\Gamma_0} + k_2^0 b_2\overline{\Gamma_1}) - 2k_2^0 k_1^0 k_2^0 b_2\overline{\Gamma_1} \quad (3)$$

$$T = -(k_1^0 b_1\overline{\Gamma_0} + k_2^0 b_2\overline{\Gamma_1}) \quad (4)$$

$$\phi = (k_1^0 + k_2^0 + k_3)(k_1^0 b_1\overline{\Gamma_0} + k_2^0 b_2\overline{\Gamma_1}) - k_1^0 k_2^0 b_2\overline{\Gamma_1} \quad (5)$$

$$Y = (k_1^0 + k_2^0 + k_3) \quad (6)$$

where the symbols are defined in the appendix of part 1.[1] Under these conditions, the graphical analysis of the characteristic points can be applied for the parametrical identification of the mechanism of zinc anodic dissolution.

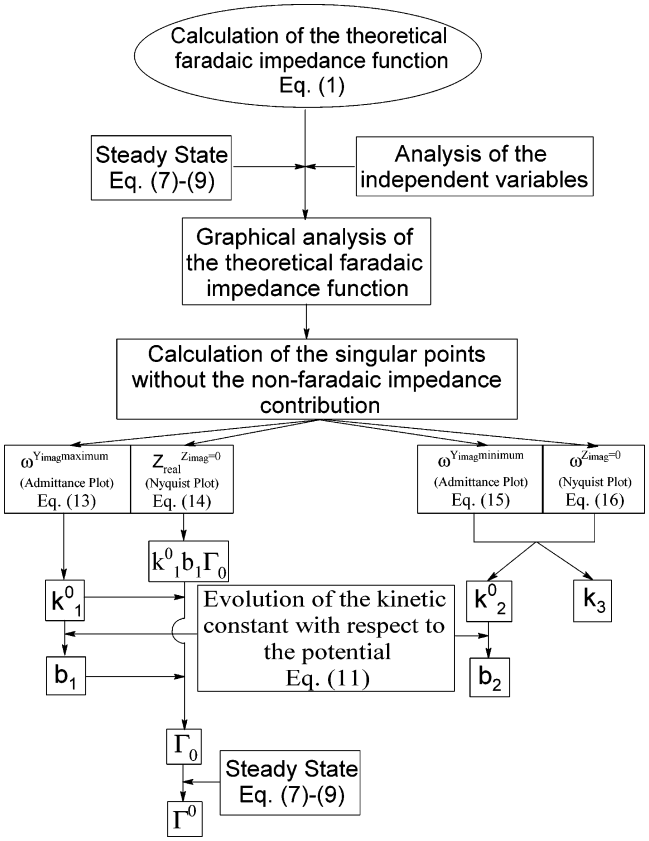

Figure 1. Flowchart of the graphical analysis by means of the characteristic points of a process that takes place through two consecutive electron transfers.

The aim of the present paper is the description of the use of the graphical analysis of the faradaic impedance function through the characteristic points of the electrochemical impedance spectroscopy (EIS) plots.[1] For that purpose, the evolution of the zinc anodic dissolution has been studied according to the steady-state potential and the roughness of the working

* Author to whom correspondence should be addressed. E-mail: Francisco.Vicente@uv.es.
[†] Universitat de València.
[‡] Université P. et M. Curie.

10.1021/jp046794b CCC: $30.25
Published on Web 02/18/2005

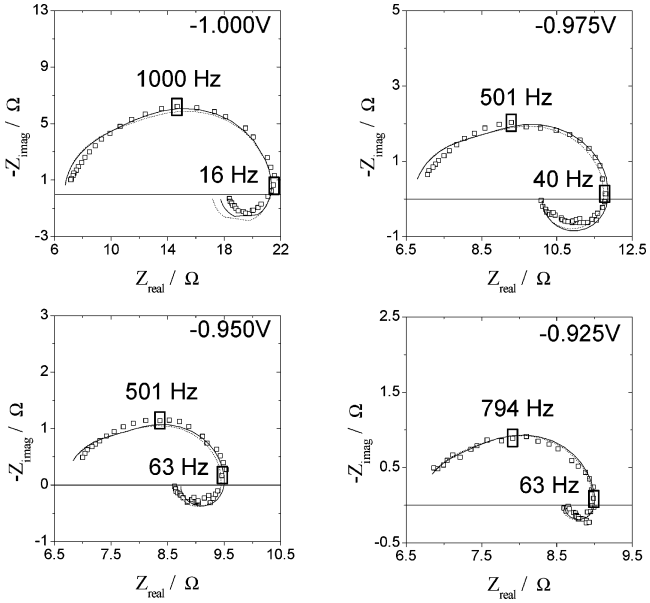

Figure 2. Dependence of the electrical impedance spectra on the steady-state potential. Experimental conditions were H_3BO_3 0.32 M, Na_2SO_4 1.32 M, NH_4Cl 0.26 M, and T 297.5 ± 0.1 K. The working solution was deaerated by bubbling argon for 5 min, and the working electrode was a shooping plate. The squares are the experimental data, the continuous lines are the spectra fitting (Table 1), and the dashed lines the spectra simulated from the kinetics parameters obtained by means of the characteristic points (Table 2).

electrode. Relevant information about this system can be obtained by analyzing these characteristic points.

Experimental Section

The electrochemical experiments were carried out with a typical three-electrode cell with a platinum plate as a counter electrode and a $Ag|AgCl|KCl_{sat}$ reference electrode. The working electrodes, with a geometrical surface area of 0.5 cm^2, were cut from galvanized steel sheets supplied by the GALESA company (Galvanizadora Valenciana S.A., Xest, Spain). Various types of galvanized plates were used as working electrodes: shooping plate (100−200 μm), hot dip galvanized steel (50−150 μm), continuous hot dip galvanized steel (20 μm), and electrogalvanized steel (5−25 μm).

The working solution was composed of H_3BO_3 (R.P. Normapur) 0.32 M, NH_4Cl (p. a. Panreac) 0.26 M, and Na_2SO_4 (Gehe &Co. A. G. Dresden) 1.33 M, pH = 4.4.[4] The cell was thermostatized at 24.4 °C by means of a HETO Denmark bath and bubbled with argon (Air Liquide S.A., U-N45) for about five minutes.

These experiments were carried out by means of a potentiostat−galvanostat PAR 273A, and the frequency analyzer was used with a lock-in-amplifier PAR 5210. The impedance measurements were made in the frequency range from 0.05 to 10^4 Hz, with a signal amplitude of 5 mV rms. Fitting of experimental data to the theoretical model proposed was done by means of a "homemade" least squares software based on the Marquardt method for optimization of functions and J. R. Macdonald weighting for the real and imaginary parts of impedance.[5,6]

Results and Discussion

Fitting to the Theoretical Impedance Function. Figure 2 shows experimental impedance data of the zinc anodic dissolution process with respect to the steady-state potential in a deaerated sulfated medium. These spectra are characterized by a capacitive loop at high frequencies followed by an inductive loop at low frequencies. Both loops decrease in diameter when the steady-state potential is shifted anodically. So, assuming that this process takes place by means of two consecutive single electron transfers in these experimental conditions,[3] the theoretical faradaic impedance function derived in the part 1 of this work,[1] eq 1, can be used to explain the impedance with respect to the steady-state potential.

The experimental data are fitted to eq 1 considering the following hypothesis:

1. The contribution to the system impedance of the nonfaradaic current and of the ohmic drop in the solution are simulated by a double layer capacitance in parallel and a series resistance respectively.[7,8]

2. Should the faradaic system be at its steady state, the mean values of the surface concentrations are given by

$$\overline{\Gamma_0} = \frac{k_2^{\,0} k_3}{k_1^{\,0} k_2^{\,0} + k_1^{\,0} k_3 + k_2^{\,0} k_3} \Gamma^0 \tag{7}$$

$$\overline{\Gamma_1} = \frac{k_1^{\,0} k_3}{k_1^{\,0} k_2^{\,0} + k_1^{\,0} k_3 + k_2^{\,0} k_3} \Gamma^0 \tag{8}$$

$$\overline{\Gamma_2} = \frac{k_1^{\,0} k_2^{\,0}}{k_1^{\,0} k_2^{\,0} + k_1^{\,0} k_3 + k_2^{\,0} k_3} \Gamma^0 \tag{9}$$

where Γ^0 is the surface concentration of the active sites. Also, due to the steady state, the kinetic rates obey the following equalities

$$k_1^{\,0} \overline{\Gamma_0} = k_2^{\,0} \overline{\Gamma_1} = k_3 \overline{\Gamma_2} \tag{10}$$

The methodology followed to obtain kinetic parameters from the fitting of experimental data to the impedance function is summarized in the flowchart of Figure 3. This procedure takes into account the fact that the theoretical impedance function only depends on seven independent parameters: the electrolyte resistance, the double layer capacitance, the three kinetic constants, and the two products of the two exponential factors of these constants by the surface concentration of active sites ($b_1\Gamma^0$ and $b_2\ \Gamma^{\,0}$), since the variables b_i and Γ^0 always appear factorized in the impedance function, eq 1.

Figure 2 shows the simulated curves obtained from the fitting of experimental data to eq 1. The kinetic parameters provided by these fittings are shown in Table 1. In this table, it could be noticed that both the electrolyte resistance and the double layer capacitance remain almost constant with respect to the steady-state potential in these experimental conditions. This is due to the fact that the same electrode is used for all of the series of measurements and that the range of potentials explored is rather narrow.

The preexponential factors of the kinetic constants and their dependence on the potential are shown in Figure 4. According to this figure, it can be considered that the kinetic constants corresponding to electron transfers obey a Butler−Volmer law, eq 11.

$$k_i^{\,0} = \overline{k_i}\, e^{b_i E} \tag{11}$$

where

$$b_i = \frac{n_i \alpha_i F}{RT} \tag{12}$$

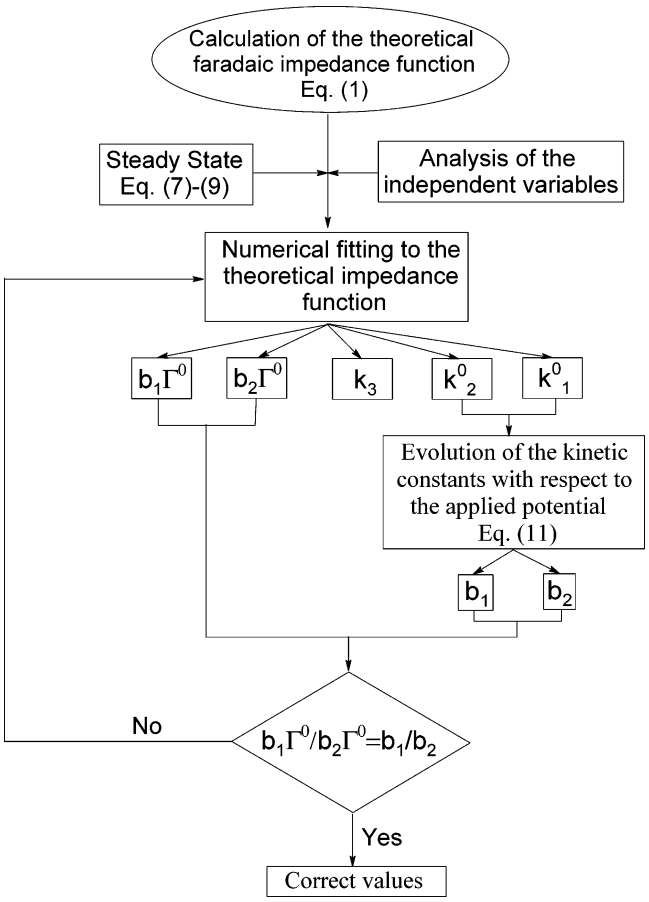

Figure 3. Flowchart of the EIS fitting from the theoretical faradaic impedance function, eq 1.

TABLE 1: Kinetic Parameters Calculated from the Fitting of the Experimental Data of Figure 2

E (V)	k_1^0 (s^{-1})	k_2^0 (s^{-1})	k_3 (s^{-1})	Γ^0 (mol m^{-2})	R_u (Ω)	C_{dl} (F m^{-2})
−0.900	14 000	15	27	0.00051	6.7	0.78
−0.925	10 000	15	27	0.00051	6.7	0.84
−0.950	6300	9.2	27	0.00060	6.7	0.84
−0.975	4000	5.3	27	0.00050	6.7	0.72
−1.000	2400	4.6	12	0.00024	6.7	0.60

That way, the parameters b_i are evaluated from the dependence of k_i^0 on the potential, and as a result, the transfer coefficients are deduced from eq 12. The transfer coefficients are 0.46 and 0.36 for the first faradaic and the second faradaic transfers, respectively. The kinetic constant associated with the transport step does not depend on the potential, as could be expected for a chemical process.

In Figure 4, the controlling step of the faradaic process is also established according to the steady-state potential. So, the zinc anodic dissolution in these experimental conditions is controlled by the second faradaic transfer at steady-state potentials more cathodic than −0.90 V, whereas the transport step is the controlling step at steady-state potentials more anodic than −0.90 V.

This variation in the rate determining step is also observed in the shape of the EIS plots; the system presents an inductive loop at low frequencies at steady-state potentials more cathodic than −0.90 V, while the inductive loop disappears at steady-state potentials more anodic than −0.90 V. It is possible to say that the inductive loop is characteristic for a control by the electron transfer.[9,10]

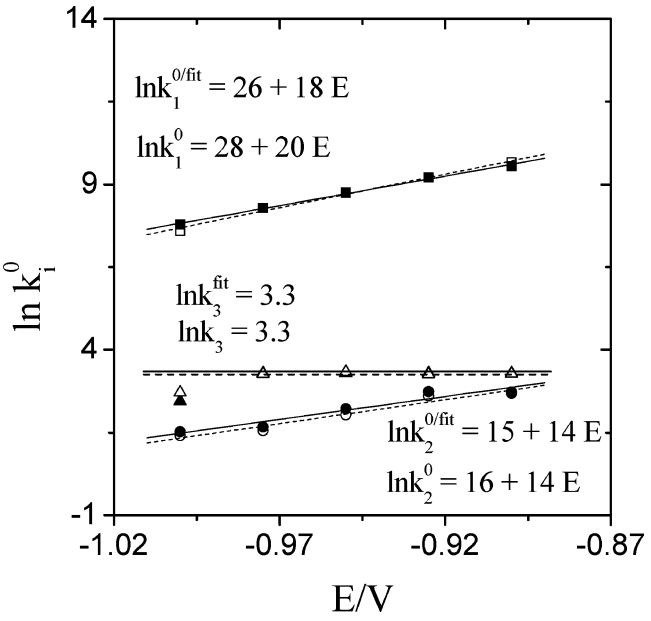

Figure 4. Curve of the preexponential factors of the kinetics constants, k^0_i, vs the steady-state potential, E: ln k^0_1 (□), ln k^0_2 (○), and ln k_4 (△). The white figures are the kinetic parameters calculated by means of EIS simulations (Table 2), the black figures the kinetics parameters calculated by means of EIS fittings (Table 1), the dashed lines are the exponential fittings of the parameters of the EIS simulations, and continuous lines are the exponential fittings of the parameters of the EIS fittings.

The estimation of b_i by means of the previous fittings also allows us to calculate the surface concentration of active sites, since the value b_i Γ^0 is a parameter obtained from this EIS fittings. Table 1 shows the values of these surface concentrations. These values keep constant in the studied potential range, as it could be expected.

In the parametrical identification procedure, the kinetic parameters calculated at −1.000 V are affected by a large uncertainty, since, at this potential, the hydrogen evolution and the zinc reduction take place at the same time as the zinc anodic dissolution.

Characteristic Points of EIS Plots in the Complex Plane. Although the fitting procedure for obtaining kinetic parameters is absolutely valid, there are other possibilities for obtaining an estimation of these parameters, such as the use of parametrical identification procedure from the characteristic points of the EIS spectra, eqs 13−16 and the flowchart of Figure 1.

$$\omega^{Y_{imag}\text{maximum}} \overset{k_1^0 \gg k_2^0, k_3}{\approx} k_1^0 \tag{13}$$

$$FAZ^{Z_{real}=0} \overset{k_1^0 \gg k_2^0, k_3}{\approx} \frac{1}{k_1^0 b_1 \overline{\Gamma_0}} \tag{14}$$

$$\omega^{Y_{imag}\text{minimum}} \overset{k_1^0 \gg k_2^0, k_3}{\approx} (k_3 + k_2^0) \tag{15}$$

$$\omega^{Z_{imag}=0} = \sqrt{k_1^0 (k_3 - k_2^0)} \tag{16}$$

It is interesting to note that, according to eq 16, there is no intercept point if $k_3 < k_{20}$. This point has been analyzed and discussed in part 1.[1]

In the experimental calculation of the characteristic points, the contributions of the electrolyte resistance and the double layer capacitance to the electrical impedance should be con-

TABLE 2: Evolution with Respect to the Steady State Potential of Characteristic Points of the Impedance Function of the Zinc Anodic Dissolution in Deaerated Sulfated Medium and Their Kinetic Parameters[a]

E (V)	$\omega^{Y_{imag}maximum}$ (rad s^{-1})	$Z_{real}^{Z_{imag}=0}$ (Ω)	$\omega^{Y_{imag}minimum}$ (rad s^{-1})	$\omega^{Z_{imag}=0}$ (rad s^{-1})	k_1^0 (s^{-1})	k_2^0 (s^{-1})	k_3 (s^{-1})	Γ^0 (mol m^{-2})
−0.900	16 000	2.4	41	430	16000	15	26	0.00045
−0.925	10 000	2.3	40	350	10000	14	26	0.00050
−0.950	6000	2.8	36	360	6300	7.6	28	0.00061
−0.975	4000	5.1	31	290	4000	4.7	26	0.00050
−1.000	2000	14.8	19	150	2000	4.1	15	0.00022

[a] The impedance dates shown in this table have been corrected with the values of the electrolyte resistance and the double layer capacitance shown in Table 1.

TABLE 3: Evolution with Respect to the Steady State Potential of Characteristic Points of the Direct Parametrical Identification Procedure and the Kinetic Parameters Calculated in Table 2[a]

E/V	$\omega^{Y_{imag}maximum}$ (rad s^{-1})	$\omega^{Y_{imag}minimum}$ (rad s^{-1})	$\omega^{Z_{imag}maximum}$ (rad s^{-1})	$C_{real}^{C_{real}maximum}$ (μF)	k_1^0 (s^{-1})	k_2^0 (s^{-1})	k_3 (s^{-1})	$b_2\overline{\Gamma_0}$ (mol m$^{-2}V^{-1}$)
−0.900	16 000	41	47	10	16 000	15	26	4×10^{-6}
−0.925	10 000	40	47	20	10 000	14	26	6×10^{-6}
−0.950	6000	36	47	30	6300	7.6	28	8×10^{-6}
−0.975	4000	31	44	20	4000	4.7	26	7×10^{-6}
−1.000	2000	19	24	23	2000	4.1	15	5×10^{-6}

[a] The impedance data shown in this table are corrected for the electrolyte resistance and the double layer capacitance with the values shown in Table 1.

sidered. Kinetic parameters obtained by means of this parametrical identification procedure are shown in Table 2. These parameters allow the simulation of the EIS experimental spectra by means of eq 1 (Figure 2).

As can be observed in Figure 2, the EIS spectra simulation from the characteristic points agrees with the experimental data and the simulation from the kinetic parameters obtained from the EIS fittings.

Figure 4 shows the evolution with respect to the steady-state potential of the preexponential factors of the kinetic constants of the zinc anodic dissolution process. These values are fairly similar to the kinetic values obtained by means of the EIS fittings (Figure 4). Thus, the conclusions obtained for the reaction mechanism are the same as the conclusions obtained by means of these fittings. The graphical analysis through the characteristic points is a fast, simple, and accurate method of determination of the kinetic parameters.

It could be also interesting to analyze the dependence of some of the characteristics points measured directly from EIS plots. Hence, there are some very interesting points that provide a quasi-direct access to the kinetic parameters. Some of these points are

$$\omega^{Z_{imag}maximum} \overset{k_1^0 \gg k_2^0, k_3}{\approx} (k_3 + k_2^0) + (k_3 - k_2^0)\frac{b_2}{b_1} \overset{b_2=b_1}{=} 2k_3 \quad (17)$$

$$\frac{C_{real}^{C_{real}maximum}}{FA} \overset{k_1^0 \gg k_2^0, k_3}{\approx} b_2\overline{\Gamma_0} \quad (18)$$

As commented above, the parameter $\omega^{Y_{imag}maximum}$, eq 13, also provides directly the kinetic parameter k_1^0, whereas, on the other hand, the parameter $\omega^{Y_{imag}minimum}$, eq 15, provides a quasi-direct method to determine the kinetic constant of the second electron transfer from the value of $\omega^{Z_{imag}maximum}$, eq 17. As a result, the kinetic parameters of this electrodic system can be estimated directly from the EIS plots.

Table 3 shows the values of these characteristic points by comparison to the values of the kinetic parameters calculated by means of the EIS fittings. As can be observed in this table and has been predicted above, these points are a quasi-direct estimation about the kinetic parameters of this electrodic system.

In this direct procedure of parametrical identification, the parameters b_i can be considered equal at the beginning of the identification procedure and, later on, can be calculated through the evolution of the kinetic constants with respect to the potential, as commented above in eq 11. Thus, the kinetic parameters can be recalculated considering the correct values of the b_i parameters.

This latter iterative procedure of parametrical identification allows us to calculate the kinetic parameters of this electrochemical mechanism without the determination of the whole EIS spectra. Therefore, the electroactive surface may be polarized for a time reduced by about 25%. Consequently, this method would be well-suited for studying thin coated galvanized steel, thus avoiding a total stripping away of the zinc layer. More generally, this method allows us to minimize the drawback in the EIS technique due to the time dependence of the interface.

A Practical Application of the Direct Measure on the EIS Spectra: Characterization of Different Kinds of Galvanized Steels. The dependence of the characteristic point $\omega^{Z_{imag}minimum}$ on the steady-state potential is simulated in Figure 5. This simulation is carried out by means of the kinetic parameters interpolated from Figure 4 and the theoretical expression of $\omega^{Z_{imag}minimum}$, eq 19. Asexpected, this simulation agrees with the experimental data. Therefore, the methodology of characteristic points can be considered appropriate for the study of the electrode processes that take place through two consecutive single electron transfers.

$$\omega^{Z_{imag}minimum} \overset{k_1^0 \gg k_2^0, k_3}{\approx} \frac{k_1^0}{1 + \frac{b_2}{b_1}} \quad (19)$$

Another possible applicability of this graphical analysis can be found in eq 1, which establishes the way the impedance depends on the electroactive surface area of the working electrode. Taking into account that roughness is related with electroactive surface, this equation may serve to obtain an estimation for the roughness of the working electrode.

In a previous paper,[11] the quantitative ratio between the roughness of the working electrode and the impedance is established easily, eq 21, by means of the fractal dimension[12]

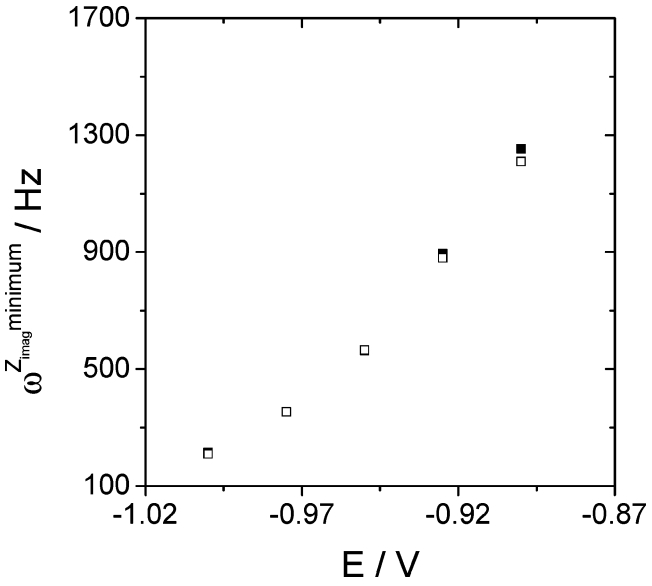

Figure 5. Evolution of the characteristic point $\omega^{Z_{imag}\text{minimum}}$ with respect to the steady-state potential. The white figures are the experimental data, and the black figures are the simulated data from the kinetic parameters of Table 1.

TABLE 4: Evolution of the Same Characteristic Points with Respect to the Fractal Dimension of the Working Electrode[a]

working electrode	fd	$\omega^{\text{minimum }\omega\uparrow}$ (Hz)	$\omega^{\text{maximum }\omega\downarrow}$ (Hz)
continuous hot dip galvanized steel	2.44	470	6.2
hot dip galvanized steel	2.59	480	6.3
electro-galvanized steel	2.62	470	6.2
shooping plate	2.96	470	6.3

[a] The values of the fractal dimension are obtained from the bibliography.[11]

of the working electrode and the characteristic point in which the imaginary part of impedance is equal to zero,[1] $Z_{real}^{Z_{imag}=0}$ eq 14, since the fractal dimension is related with the surface area, *A*, through the scaling law,[13] eq 20.

$$A(\lambda) = A_0\lambda^{-(\text{fd}-2)} \tag{20}$$

$$\text{fd} = 2 + \frac{\ln(FA_0 Z_{real}^{Z_{imag}=0} k_1^{\,0} b_1 \overline{\Gamma_0})}{\ln \lambda} \tag{21}$$

where λ is the scaling ratio, fd is called the fractal dimension of the surface, and A_0 is the geometrical surface area of the working electrode.

If the kinetic constants are not dependent on the roughness of the working electrode, then the frequency of the minimum at high frequencies of the Bode *C* plot[1] and the frequency of the maximum of the Bode *Z* plot (as is observed in eqs 22 and 23) must remain constant with the variation of the roughness of the working electrode. This behavior was actually observed as shown in Table 4. Thus, the theoretical value of the minimum of the Bode *C* plot corresponds to a theoretical frequency of 470 Hz, and the maximum of Bode *Z* plot corresponds to a theoretical frequency of 6.3 Hz; both theoretical values agree with the experimental values shown in Table 4 (taking into account the experimental error in the calculation of the double layer capacitance). These experimental values corroborate the relations with the kinetic parameters established at both characteristic points and the nondependence of the kinetic constants on the roughness of the working electrode.

$$\omega^{\text{minimum }\omega\uparrow} \overset{k_1^0 \gg k_2^0, k_3}{\approx} \sqrt{\frac{k_1^{\,0^2} b_1}{b_1 + b_2}} \overset{b_1 = b_2}{=} \frac{k_1^{\,0}}{\sqrt{2}} \tag{22}$$

$$\omega^{\text{maximum }\omega\downarrow} \overset{\substack{k_1^0 \gg k_2^0, k_3 \\ k_3^0, k_{-1}^0 \to 0}}{\approx} \sqrt{\frac{(k_3 + k_2^{\,0})((k_3 + k_2^{\,0})b_1 + (k_3 - k_2^{\,0})b_2)}{b_1}} \tag{23}$$

The dependence or nondependence of these characteristic points on the roughness of the working electrode and on the steady-state potential confirms the study of the electrochemical systems (which takes place through two consecutive single electron transfers) by means of the characteristic points as well as the parametrical identification procedure by means of these characteristic points (Figure 1).

Taking that into account, the graphical analysis of this theoretical model can also be used to understand the evolution of the zinc anodic dissolution with regard to other experimental parameters, such as the pH.[14] At acid pH, this electrochemical system only displays two consecutive capacitive loops, whereas, when the pH increases, these loops are transformed into a capacitive loop at high frequencies followed by an inductive loop at low frequencies. This fact can be explained by the participation of the hydroxyl ions in the second faradaic transfer, decreasing the rate of this faradaic transfer, since these ions can stabilize the monovalent zinc on the surface of the working electrode.

In chloride solutions, this electrodic system presents only two consecutive capacitive loops;[15,16] this fact can be explained by considering that k_3 is lesser than k_2 and, therefore, that the rate of the transport step is lesser than the rate of the second electronic transfer at these experimental conditions. Other solutions that present the same electrochemistry plots[16] can be also explained by means of the same hypothesis.

It is possible to say that this theoretical model can explain easily and quickly the EIS spectra of the electrodic systems (which takes place through two consecutive single electron transfers) in different experimental conditions. Furthermore, it is also possible to say that this graphical method has a very high accuracy on the calculation of the kinetic parameters.

Conclusion

The graphical analysis by means of the characteristic points provides an easy and fast method for parametrical identification and, consequently, an easy and fast method for simulation of the EIS spectra. As a result, it is possible to say that a wealth of information concerning this kind of electrochemistry mechanism can be obtained accurately by using this kinetic model and the graphical analysis of some of the characteristic points of the EIS spectra.

Considering these characteristic points, the direct procedure of parametrical identification of the characteristic points also allows us to reduce the number of frequencies measured in the performance of the impedance experiments, with the consistent decrease in the perturbation time of the electroactive surface and, therefore, with the consistent increase of the applicability of EIS to time-dependent systems.

Acknowledgment. This work has been supported by CICyT-MAT/2000-0100-P4. D. Giménez-Romero acknowledges a fellowship from the Generalitat Valenciana, Program FPI. J. J. García-Jareño acknowledges the financial support by the "Ra-

món y Cajal" program (Ministerio de Ciencia y Tecnologia, Spanish Ministry of Science and Technology).

References and Notes

(1) Garcia-Jareño J. J.; Gimenez-Romero D.; Keddam M.; Vicente F. *J. Phys. Chem. B.* **2005**, *109*, 4584.
(2) Wiart R. *Electrochim. Acta* **1990**, *35*, 1587.
(3) Giménez-Romero D.; García-Jareño J. J.; Vicente F. J. *Electroanal. Chem.* **2003**, *538*, 25.
(4) Ohtsuka T.; Komori A. *Electrochim. Acta* **1998**, *43*, 3269.
(5) Macdonald J. R. *Solid State Ionics* **1992**, *58*, 97.
(6) Vicente F.; Roig A.; García Jareño J. J.; Sanmatías A. Procesos electródicos del Nafión y del Azul de Prusia/Nafion sobre electrodo transparente óxido de Indio-Estaño: Un modelo de electrodos multicapa. Ed. Moliner 40, Burjassot, 2001.
(7) Prokopowiz A.; Opallo M. *Solid State Ionics* **2003**, *157*, 209.
(8) Devos O.; Aaboubi O.; Chopart JP.; Merienne E.; Olivier A.; Gabrielli C.; Tribollet B. *J. Phys. Chem. B* **1999**, *103*, 496.
(9) Itagaki M.; Shimoda K.; Watanabe K. *Electrochemistry* **2002**, *70*, 595.
(10) Giménez-Romero D.; García-Jareño J. J.; Vicente F. *J. Electroanal. Chem.* **2004**, *572*, 235.
(11) Giménez-Romero D.; García-Jareño J. J.; Vicente F. *Electrochem. Comm.* **2004**, *6*, 148
(12) Bortels L.; Van den Bossche B.; Deconinck J.; Vandeputte S.; Hubin A. *J. Electroanal. Chem.* **1997**, *429*, 139.
(13) Wang Y. B.; Yuan R. K.; Willander M. *Appl. Phys. A* **1996**, *63*, 481.
(14) Magaino S.; Soga M.; Sobue K.; Kawaguchi A.; Ishida N.; Imai H. *Electrochim. Acta* **1999**, *44*, 4307.
(15) Kalinauskas P.; Valsiunas I.; Samuleviciene M.; Juzeliunas E. *Corros. Sci.* **2001**, *43*, 2083.
(16) Hassan. H. H. *Appl. Surf. Sci.* **2001**, *174*, 201.